Dalton Transactions

ROYAL SOCIETY OF CHEMISTRY

PAPER

Published on 23 July 2026
Licensed under CC-BY-NC 4.0

Check for updates

Cite this: *Dalton Trans.*, 2026, **55**, 11833

Heterobimetallic Ln–Zn (Ln = Eu, Gd) complexes with interesting second order nonlinear optical properties

Alessia Colombo, [a] Claudia Dragonetti, *[a] Francesco Fagnani, [a] Dominique Roberto, [a] Daniele Marinotto, [b] Anna L. Pellegrino, *[c] Francesca Lo Presti,[c] Patrizia Rossi, [d] Martina Lippi[d] and Graziella Malandrino [c]

Second-order nonlinear optical chromophores based on coordination compounds offer an interesting route to enhance molecular hyperpolarizability through low-energy charge-transfer excited states and the tunable donor/acceptor character of metal centers. While lanthanide complexes are widely explored for luminescence and magnetism, their second-order NLO properties remain comparatively underinvestigated, and cationic lanthanide systems have, to the best of our knowledge, not been explored. In this context, we designed and synthesized in a simple and rapid way two new lanthanide complexes based on a europium cation or gadolinium cation and the same zinc anion: $[Eu(hfa)_2(tetrag)]^+\cdot[Zn(hfa)_3]^-$ and $[Gd(hfa)_2(tetrag)]^+\cdot[Zn(hfa)_3]^-$. Structural and spectroscopic characterization confirms the formation of well-defined cation–anion assemblies in which the lanthanide β-diketonate cation is counterbalanced by a zinc anion counterpart. The second-order nonlinear optical response was evaluated in solution by means of the Electric-Field Induced Second Harmonic generation (EFISH) technique which affords $\mu\beta_{EFISH}$ values. Both compounds present values much higher than that of the benchmark Disperse Red One, rendering them of particular interest for future applications such as in electro-optic modulators.

Received 5th March 2026,
Accepted 1st July 2026

DOI: 10.1039/d6dt00543h

rsc.li/dalton

1. Introduction

The design and synthesis of chromophores with second-order nonlinear optical (NLO) properties have gained considerable attention thanks to their variety of applications in different fields such as electro-optical devices, optical communications and optical data processing.[1,2]

To show relevant second-order NLO properties, a chromophore must be noncentrosymmetric, have a great difference between the excited state and the ground state dipole moment and show charge-transfer transitions at relatively low energy. Typically, organic molecules containing electron-withdrawing and electron-donor groups connected by a polarizable π-conjugated bridge show a good NLO response.[3–5]

In the perspective of finding active NLO-phores, it appeared that the second-order NLO response of various π-delocalized nitrogen donor ligands can be greatly enhanced upon coordination to a metal moiety which can act as electron-donor or electron-acceptor depending on its oxidation state and ancillary ligands. In the last two decades, many coordination compounds, characterized by low energy excited states of the type ligand-to-metal, metal-to-ligand, ligand-to-ligand and intraligand charge-transfer (LMCT, MLCT, LLCT, and ILCT, respectively), have shown their great potential for second-order nonlinear optics.

Coordination complexes with a large variety of metals have been studied.[6–24] Several studies have extensively investigated the nonlinear optical properties of a wide range of metal complexes.[6–10,18] Furthermore, a number of contributions have been specifically devoted to particular classes of metal-based compounds, such as ruthenium complexes,[11,14,17] platinum complexes,[12,14,19] iridium complexes,[13] ferrocene derivatives,[15,22,24] zinc complexes,[16,20] and copper complexes.[20,21,24] These works highlight the continuous interest in tailoring the optical response through metal-centered design. However, surprisingly, although lanthanide complexes have been intensively investigated for their luminescent and magnetic properties,[25,26] and for biological purposes,[27–31] there are only a few reports on their interesting NLO properties[32–41] including a recent paper by some of us.[42] Recently, an emerging class of heterobimetallic 3d–4f ionic complexes designed with cobalt

[a]*Dipartimento di Chimica, Università degli Studi di Milano and INSTM UdR Milano, Milan, Italy. E-mail: claudia.dragonetti@unimi.it*
[b]*Istituto di Scienze e Tecnologie Chimiche (SCITEC) "Giulio Natta", Consiglio Nazionale delle Ricerche (CNR), via C. Golgi 19, I-20133 Milan, Italy*
[c]*Dipartimento di Scienze Chimiche, Università di Catania and INSTM UdR Catania, Catania, Italy. E-mail: annalucia.pellegrino@unict.it*
[d]*Dipartimento di Ingegneria Industriale, Università degli Studi di Firenze, Firenze, Italy*

and rare-earth (RE = Dy, Eu, Y) metals has been synthesized and investigated for their intriguing optical and magnetic properties.[43]

Concerning the NLO properties, dipolar lanthanide complexes as $[LLn(NO_3)_3]$ (L = dibutylaminophenyl-functionalized annelated terpyridine) were reported to show a good second-order NLO response, measured by the HLS (Harmonic Light Scattering) technique in solution,[44,45] which increases when the number of f electrons increases.[32,34]

Likewise, the increase of the quadratic hyperpolarizability, β_{HLS}, of $Na_3[Ln(pyridyl\text{-}2,6\text{-}dicarboxylate)_3]$ along the lanthanide's series can be explained by the increased number of f electrons:[33] this unexpected fact was attributed to the polarization of the 4f electrons.[35] Moreover, it was reported that the quadratic hyperpolarizibilities of lanthanides complexes with nonadentate ligands based on triazacyclononane, functionalized with pyridyl-2-phosphinate groups, showed a bell-shaped trend reaching a maximum around the center of the lanthanide series.[38]

In parallel, some of us studied the second-order nonlinear optical response of $[Ln(hfa)_3(diglyme)]$ (hfa = hexafluoroacetylacetonate; diglyme = bis(2-methoxyethyl)ether) combining two different techniques in solution: EFISH (Electric-Field Induced Second Harmonic generation) and HLS, confirming the role of f electrons in controlling the second-order NLO properties.[37] The molecular quadratic hyperpolarizabilities measured by the EFISH method,[46] β_{EFISH}, initially increase rapidly with the number of f electrons, whereas the increase is much lower for the last seven f electrons; additionally, the β_{HLS} values increase, but much less rapidly, along the Ln series.[37] Similarly, the β_{EFISH} values of trinuclear lanthanide adducts $[Ln(NO_3)_3(CuL)_2]$ (Ln = La, Ce, Sm, Eu, and Er; L = *N*,*N*0-1,3-propylen-bis(salicylideniminato)) are significantly influenced by the number of f electrons: the values initially increase rapidly with the number of f electrons, when europium is used as Ln ion the increase is less marked adding other f electrons, with the β_{EFISH} value of the Er complex (11 f electrons) being only 1.1 times higher than that of the Eu complex (6 f electrons).[40] This is a confirmation that the polarizable character of f electrons is the origin of the NLO properties. As general trend, the increase of the second-order NLO response is significant up to fulfilment of half f shell, while it becomes much less relevant with the addition of further f electrons.[40] This observation and the fact that lighter lanthanides (from cerium to europium) are more abundant than the heavier ones, and are generally less expensive,[47] render europium complexes of particular interest for NLO studies.

Recently, some of us found that two luminescent β-diketonate europium complexes $[Eu(hfa)_3(1,10\text{-phenanthroline})]$ and $[Eu(tta)_3(1,10\text{-phenanthroline})]$ (hfa = hexafluoroacetylacetonate, tta = thenoyltrifluoroacetone), showed an unexpected large NLO response,[42] much higher than that previously reported for the related $[Eu(hfa)_3(diglyme)]$,[37] as evidenced by the EFISH technique in solution.[42]

To our knowledge, up to now, no cationic lanthanide complex has been studied for its second-order nonlinear properties. This observation prompted us to prepare new lanthanides complexes, formed by an europium cation and a zinc anion: $[Eu(hfa)_2(tetrag)]^+\cdot[Zn(hfa)_3]^-$ and $[Gd(hfa)_2(tetrag)]^+\cdot[Zn(hfa)_3]^-$ (tetrag = tetraethylene glycol dimethyl ether), namely complex **Eu–Zn** and complex **Gd–Zn** (Fig. 1). It turned out that these novel complexes show both interesting luminescent and/or second-order NLO properties, opening a promising route for easily prepared multifunctional NLO-active lanthanide complexes.

2. Results and discussion

Both the heterobimetallic ionic complexes $[Eu(hfa)_2(tetrag)]^+\cdot[Zn(hfa)_3]^-$ and $[Gd(hfa)_2(tetrag)]^+\cdot[Zn(hfa)_3]^-$, have been obtained through a facile one-pot synthesis starting from acetate salts and ligands in dichloromethane suspension following the general reaction (Ln = Eu and Gd):

$$Ln(CH_3COO)_3\cdot 4H_2O + Zn(CH_3COO)_2\cdot 2H_2O + 5Hhfa + tetraglyme \rightarrow [Ln(hfa)2(tetrag)]^+\cdot[Zn(hfa)_3]^- + 6H_2O + 5CH_3COOH$$

The synthetic procedure is analogous to the one reported in ref. 43 for the cobalt based complexes $[Co(hfa)_2]^-\cdot[RE(hfa)2tetraglyme]^+$ (RE = Dy, Eu, and Y). The single step synthesis uses commercially available chemicals and represents an easy and low-cost strategy to produce this type of heterobimetallic complexes with reaction yields in the 80–88% range. An excess of the two metal acetates promotes easy isolation of the adducts, as the acetate excess is insoluble and thus easily filterable. Both the complexes can be handled in air, are non-hygroscopic and soluble in common organic solvents such acetone, dichloromethane and ethanol.

2.1 Compositional and structural characterization

The atomic compositions of the complexes have been investigated through energy dispersive X-ray (EDX) analysis and

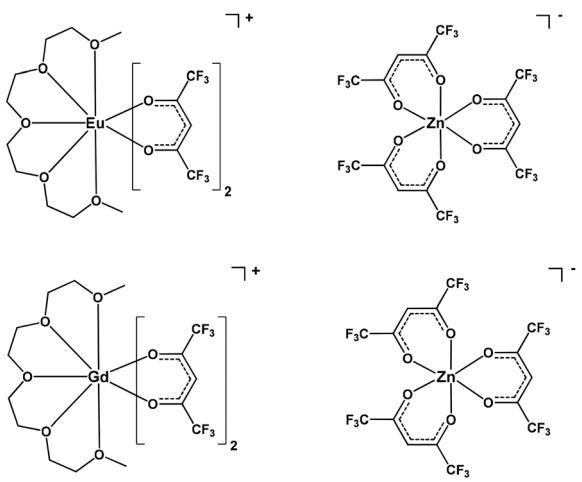

Fig. 1 Molecular formula of **Eu–Zn** and **Gd–Zn** complexes.

This journal is © The Royal Society of Chemistry 2026

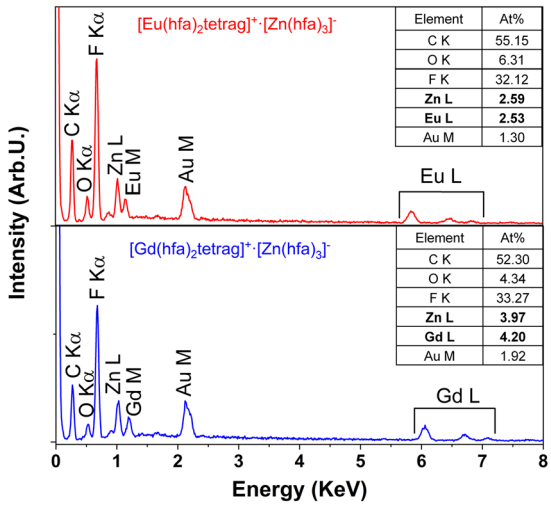

Fig. 2 EDX spectra and quantitative analyses of **Eu–Zn** and **Gd–Zn** complexes.

reported in Fig. 2. For both the compounds, the quantitative analyses confirm the stoichiometry of 1 : 1.02 for the Eu : Zn ratio and 1 : 1.05 for the Gd : Zn one. The signals at 0.27 keV, 0.53 keV and 0.68 keV, due to the K_α lines of carbon, oxygen and fluorine, respectively, come from the ligands hfa and tetraglyme of the complexes. The Au signal arises from the Au layer sputtered on the on the crystalline powder before the analyses in order to ensure a conductive material.

The structural characterization has been performed through FT-IR analyses reported in Fig. 3 with the aim of evaluating the ligands coordination to the metal centers.

In both spectra, the nujol peaks are present at 2929 cm^{-1}, 2860 cm^{-1}, 1460 cm^{-1} and 1368 cm^{-1}.

The peaks in the range of 2900 cm^{-1} are linked also to the stretching of –CH groups of tetraglyme, but it is overlapped to the nujol. The coordination of tetraglyme is supported by the peaks observed in the range 800–1000 cm^{-1}. The peaks visible in the range 1580–1660 cm^{-1} are due to the stretching of C=C and C=O. In the range 1000–1350 cm^{-1} the peaks are caused by the stretching of carbon–fluorine bonds of the hfa ligand, overlapped with other peaks related to carbon–oxygen bonds of polyether.

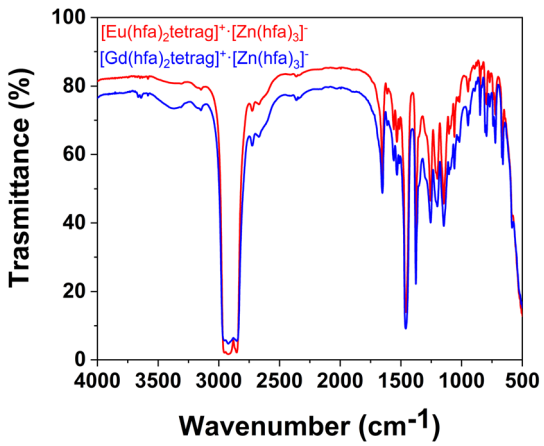

Fig. 3 FT-IR spectra of **Eu–Zn** and **Gd–Zn** complexes with nujol mulls.

2.2 Single crystal structure

The structure of heterobimetallic has been investigated through single crystal data. The crystals of both complexes were grown through low temperature solvent evaporation of their own supersaturated solution. Only the **Eu–Zn** adduct was obtained as high-quality single crystal and analyzed through single crystal diffraction. The asymmetric unit of the **Eu–Zn** complex is reported in Fig. 4.

Eu–Zn is almost isomorphous and isostructural with the already reported $[Eu(hfa)_2(tetrag)]\cdot[Co(hfa)_3]$ (**Eu–Co** in the following) and $[Y(hfa)_2(tetrag)]\cdot[Co(hfa)_3]$ (**Y–Co** in the following) salts.[37] In the asymmetric unit of **Eu–Zn** one $[Eu(hfa)_2(tetrag)]^+$ cation and one $[Zn(hfa)_3]^-$ anion are present.

In the cation, the Eu(III) atom is nine-coordinated by the oxygen atoms of two hfa anions and by the five oxygen atoms of one tetraglyme molecule (see Fig. 4). The tetraglyme molecule takes on a typical geometry, with *anti* and *gauche* orientations around the C–O and C–C bonds, respectively. This molecule wraps around the europium atom in a meridional plane, while the two hfa anions on the opposite sides of this plane (see Fig. 5).

The resulting coordination polyhedron is a distorted capped square antiprism, with the oxygen atoms O7, O8, O10, O14 and O9, O11, O12, O13 defining the two parallel squares and O15 capping this last square (see Fig. 5).

This disposition of the three ligands, as well as the resulting coordination polyhedron, are the same observed, not only in the above reported **Eu–Co** and **Y–Co** compounds, but also in the seven structures (containing a nine-coordinated metal complexes having as ligands 2 derivatives of acetylacetonate (acac) anion and one tetraglyme molecule) found in the CSD (CSD refcodes: HAZPAZ and HAZPED,[48] JEPLUL,[49] YIHLUW[50] and YIMTUJ,[51] OFULIK and OFULUW[52]). All of them contain as metal atom Ba or Sr.

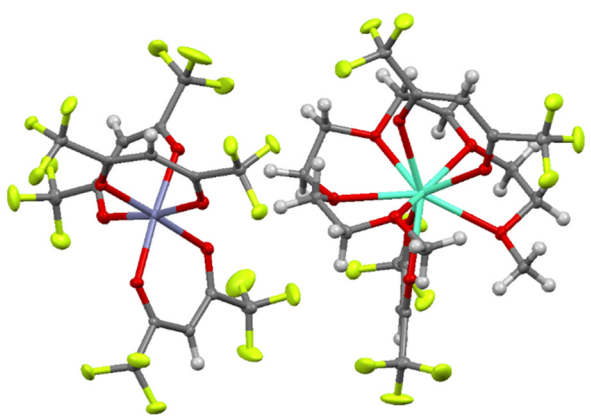

Fig. 4 ORTEP3 representation of the asymmetric unit of **Eu–Zn** (the ellipsoid probability = 30%).

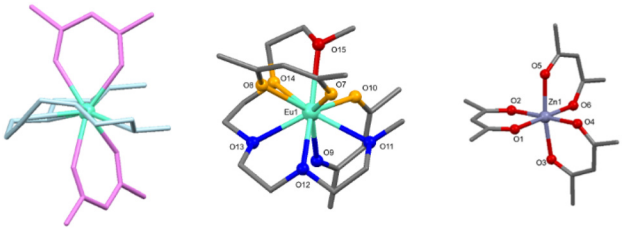

Fig. 5 View of the metal coordination geometries. Left/Middle: Eu(III) environment. In the middle panel, oxygen atoms are color-coded based on their position within the coordination polyhedron (O7, O8, O10, O14 *vs.* O9, O11, O12, O13) to better visualize the capped square antiprismatic geometry. Right: Zn(II) coordination geometry.

The Eu–O distances are all in the expected range observed in Eu complexes with oxygen as donor atom (accordingly to a search performed by using the Cambridge Structural Database, CSD v. 6.01, update November 2025).[53] As observed in the CSD, the Eu–O_{ether} are slightly longer than the Eu–O_{hfa} ones (see Table S1).

Concerning the $[Zn(hfa)_3]^-$ anion, the Zn(II) metal is hexacoordinated by the oxygen atoms of three hfa anions (see Fig. 4) giving rise to a octahedral coordination (see Fig. 5). The Zn–O distances (see Table SM-PAT-1) are in range retrieved in the CSD for Zn complexes with hfa and acac anions.

Finally, as already observed in **Eu–Co** and **Y–Co**, in the crystal packing of **Eu–Zn** layers consisting of $[Eu(hfa)_2(tetrag)]^+$ cations, oriented perpendicular to the b axis, alternating with layers containing $[Zn(hfa)_3]^-$ anions are present (see Fig. 6). No significant intermolecular interactions are seen either within the layers or between the layers.

Since no single crystals suitable for X-ray diffraction could be isolated for the **Gd–Zn** adduct, its structural characterization was performed *via* high-resolution powder X-ray diffraction (PXRD) using an Anton Paar XRDynamic 500 diffractometer (Cu-Kα1 radiation = 1.54056 Å, 40 kV × 40 mA) at room temperature (300 K).

The initial unit cell parameters were indexed using the EXPO v2.3.11 [54] software package and subsequently refined *via* full-profile refinement in DIFFRACT.TOPAS v6.[55] The refined

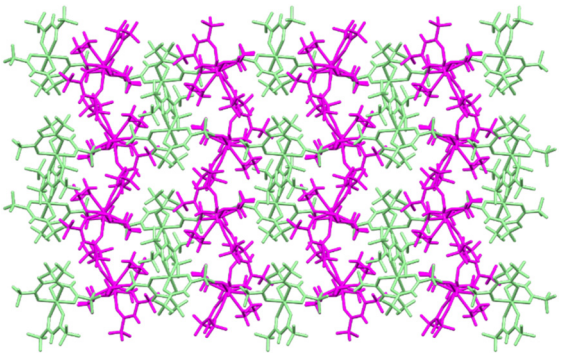

Fig. 6 Crystal packing of **Eu–Zn** view along the *a*-axis ([Eu(hfa)$_2$(tetrag)]$^+$ cation = magenta, [Zn(hfa)$_3$]$^-$ anion = pale green).

Table 1 Crystallographic data for **Gd–Zn**

Empirical formula	$C_{35}H_{27}GdF_{30}O_{15}Zn$
Formula weight	1480.17
T (K)	300
Crystal system, space group	Monoclinic, $P2_1/n$
λ (Å)	1.54184
Unit cell dimensions (Å, °)	a = 14.562(2)
	b = 23.431(4)
	beta = 94.057(3)
	c = 15.755(3)
V (Å^3)	5362(1)
Z, d_{calc} (g cm^{-3})	4, 1.833
R_{wp}	8.581%

structural and crystallographic parameters are summarized in Table 1, confirming that the **Gd–Zn** complex crystallizes in the monoclinic $P2_1/n$ space group with a satisfactory agreement factor (R_{wp} = 8.581%).

In Fig. 7, the experimental PXRD pattern of the **Gd–Zn** phase is compared with the theoretical profile simulated from the single-crystal data of the **Eu–Zn** analogue. The profiles display an excellent overall match. The slight shift toward lower 2θ angles (corresponding to a larger unit cell volume) observed for the **Gd–Zn** sample is fully consistent with lattice thermal expansion, given the 200 K temperature difference during data collection (300 K for **Gd–Zn** *versus* 100 K for **Eu–Zn**). These findings unambiguously demonstrate that the **Gd–Zn** complex is isostructural to its **Eu–Zn** counterpart, a conclusion further corroborated by the closely matching FT-IR spectroscopic data (see infra).

Crystallographic data and refinement parameters are reported in Table 1.

2.3 Linear optical properties

The absorption spectrum of the **Eu–Zn** complex, reported in Fig. 8a, displays an intense band centered at 301 nm, with a ε of 45 700 M^{-1} cm^{-1}. This band is in accordance with the typical behavior of the Eu adducts and is similar to the one

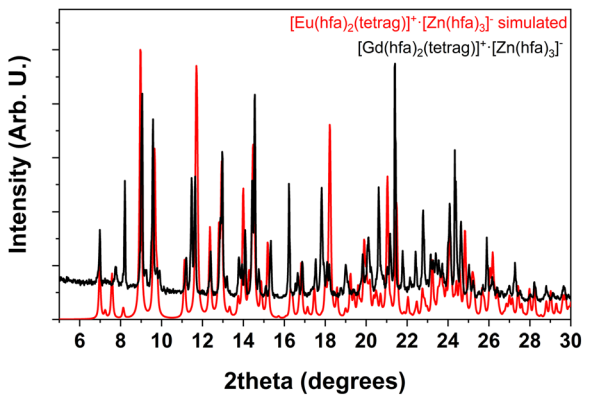

Fig. 7 Comparison between the theoretical PXRD pattern of **Eu–Zn** (red line, simulated from single-crystal data collected at 100 K) and the experimental high-resolution PXRD pattern of **Gd–Zn** (black line, collected at 300 K).

This journal is © The Royal Society of Chemistry 2026

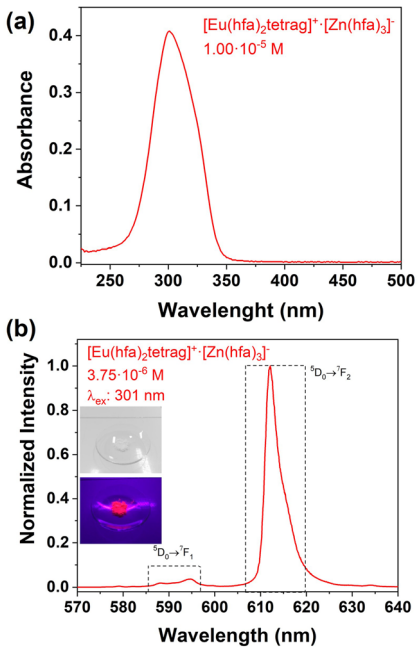

Fig. 8 UV-Vis spectrum in CH_2Cl_2 solution (a), and luminescence spectrum (λ_{exc} = 301 nm) (b) of **Eu–Zn** complex. In the inset the images of the compound with and without irradiation with UV lamp (λ: 365 nm).

found for the [Eu(hfa)$_3$(diglyme)] compound.[42] This peak can be assigned to the lowest spin-allowed π–π* transition of the β-diketonate hfa ligand.

The photophysical properties of the complex **Eu–Zn** were thoroughly investigated both in solution and in the solid state. The luminescence of the **Eu–Zn** adduct in solution, registered at room temperature using an excitation wavelength of 301 nm, is reported in Fig. 8b. The emission peaks arise from f–f emission transitions, involving the $^5D_0$ excited state to the ^7F_J multiplet of the Eu(III) ion. In particular, the peaks centered at 594 and 612 nm are assigned to the Eu ion transitions $^5D_0 \rightarrow {}^7F_1$ and $^5D_0 \rightarrow {}^7F_2$, respectively.[56] Furthermore, the asymmetry ratio between the $^5D_0 \rightarrow {}^7F_2$ and $^5D_0 \rightarrow {}^7F_1$ electronic transitions with a value of 17.07 points to a highly asymmetric environment of the Eu moiety of the adduct.

In solution, the emission quantum yield was determined to be 27.9%. In addition, the emission quantum yield was also measured for the powdered sample, yielding a lower value of 11.6% (see Fig. S1 in the SI). Luminescence lifetime measurements were carried out in both states to further characterize the excited-state dynamics. In the solid state (powder), the lifetime was found to be τ = 743 μs (Fig. S2, SI), whereas in solution the lifetime was slightly shorter, τ = 650 μs (Fig. S3, SI). Contrarily to **Eu–Zn**, the **Gd–Zn** complex is not luminescent.

2.4 Second-order nonlinear optical properties

Two techniques can be used in order to determine in solution the experimental value of the quadratic hyperpolarizability of molecular NLO chromophores: the hyper-Rayleigh scattering (HRS, also called HLS for harmonic light scattering) method and the electric field induced second harmonic generation (EFISH) method.

The HRS technique[44,45] involves the detection of the incoherently scattered second harmonic generated by the compound in solution under irradiation with a λ laser wavelength, leading to the mean value of the tensor product $\beta \times \beta$. By looking at the polarization dependence of the second harmonic signal, which is determined by selecting the polarization of the incident and scattered radiation, it is possible to obtain information about the single components of the quadratic hyperpolarizability tensor β. The HRS technique can be used for all kind of molecules (dipolar and octupolar).

The EFISH technique,[46] suitable for dipolar molecules only, provides information on the molecular NLO properties through the following equation:

$$\gamma_{\mathrm{EFISH}} = (\mu\beta_{\mathrm{EFISH}}/5kT) + \gamma\ (-2\omega;\ \omega, \omega, 0)$$

where $\mu\beta_{\mathrm{EFISH}}/5kT$ is the dipolar orientational contribution and $\gamma\ (-2\omega; \omega, \omega, 0)$ is the electronic cubic contribution, which can usually be neglected studying the second-order NLO properties of dipolar molecules. β_{EFISH} is the projection along the dipole moment axis of β_{VEC}, which is the vectorial component of the tensor of the quadratic hyperpolarizability, working with an incident wavelength λ of a pulsed laser. It is important to underline that in order to avoid overestimation of the quadratic hyperpolarizability value, due to resonance enhancements, it is necessary to work with an incident wavelength λ whose second harmonic $\lambda/2$ is far from any absorption band of the compound investigated. Besides, in order to obtain the value of β_{EFISH}, it is necessary to know the value of the ground state dipole moment μ of the molecule. However, for optoelectronic applications, the "figure of merit" is the $\mu\beta_{\mathrm{EFISH}}$ value itself. A compound with a $\mu\beta_{\mathrm{EFISH}}$ value higher than that of Disperse Red One (500×10^{-48} esu), proposed for electrooptic polymeric poled films,[57,58] can be considered of interest for photonic applications and should be maximized.

In the present work, the second-order nonlinear optical properties of complexes **Eu–Zn** and **Gd–Zn** have been investigated in chloroform solution (10^{-3} M) by means of the EFISH technique,[46] working with an incident radiation of low energy (λ = 1.907 μm), chosen to avoid resonance enhancement. The $\mu\beta_{\mathrm{EFISH}}$ values of the two complexes are reported in Table 2.

The value determined for **Eu–Zn** is similar to that previously reported for the trinuclear [Eu(NO$_3$)$_3$(CuL)$_2$] complex, where L is *N*,*N*′-1,3-propylen-bis(salicylideniminato),[40] whereas that of **Gd–Zn** is higher. Both complexes present $\mu\beta_{\mathrm{EFISH}}$ values much higher than that of Disperse Red One, so they are of particular interest for future applications such as in electro-optic modulators.

Table 2 $\mu\beta_{\mathrm{EFISH}}$ of the investigated complexes

Complex	C(M) (10^{-3} M)	$\mu\beta_{\mathrm{EFISH}}$ ($\times 10^{-48}$ esu)
[Eu(hfa)$_2$(tetrag)]$^+$·[Zn(hfa)$_3$]$^-$	$CHCl_3$	640
[Gd(hfa)$_2$(tetrag)]$^+$·[Zn(hfa)$_3$]$^-$	$CHCl_3$	815

The knowledge of the second-order NLO properties of lanthanide complexes is rather poor when compared to that of other metal complexes. As evidenced in the introduction, a few studies have been done with the HLS technique even less with the EFISH method. However, it is possible to compare the $\mu\beta_{EFISH}$ values of complexes **Eu–Zn** and **Gd–Zn** with that of the related [Eu(hfa)$_3$(diglyme)] and [Gd(hfa)$_3$(diglyme)] complexes,[37] which are characterized by β_{HLS} values among the best reported up to now.[32,34] [Eu(hfa)$_2$(tetrag)]$^+$·[Zn(hfa)$_3$]$^-$ has a $\mu\beta_{EFISH}$ value four times greater than [Eu(hfa)$_3$(diglyme)] ($\mu\beta_{EFISH}$ = 161 × 10^{-48} esu)[37] whereas [Gd(hfa)$_2$(tetrag)]$^+$·[Zn(hfa)$_3$]$^-$ is characterized by a value almost five times greater than [Gd(hfa)$_3$(diglyme)] ($\mu\beta_{EFISH}$ = 170 × 10^{-48} esu).[37] Interestingly, the increase of the NLO response observed when switching from **Eu–Zn** to **Gd–Zn** is greater than that observed in the previously reported europium and gadolinium complexes.[37]

The new heterobimetallic lanthanide complexes presented in this work represent a novel class of promising multifunctional NLO-active materials and confirms the great potential of lanthanide complexes in the field of nonlinear optics.

3. Experimental section

3.1 Reagents

Commercial europium acetate tetrahydrate, zinc acetate hydrate, gadolinium acetate hydrate, and Hhfa (1,1,1,5,5,5-hexafluoro-2,4-pentanedione) were purchased from STREM Chemicals Inc, while tetraglyme (2,5,8,11,14-pentaoxapentadecane) was purchased from Sigma-Aldrich. All chemicals were used without any further purification.

3.2 Synthetic procedures

Synthesis of [Eu(hfa)$_2$(tetrag)]$^+$·[Zn(hfa)$_3$]$^-$ (Eu–Zn). 0.72 g (2.19 mmol) of Eu(CH$_3$COO)$_2$·4H$_2$O and 0.49 g (2.25 mmol) of Zn(CH$_3$COO)$_3$·xH$_2$O were suspended in 50 ml of dichloromethane inside a flat bottom flask, and then 0.44 ml of tetraglyme (2.00 mmol) were added. The suspension was vigorously stirred at room temperature for 10 minutes. Subsequently, 1.41 ml of Hhfa (10 mmol) were added and the mixture was refluxed for 90 minutes under magnetic stirring. After filtration of the acetate excess, white crystals were obtained through evaporation of the solvent. The melting point of the obtained compound was 165–167 °C at 760 torr. Elemental analysis ($C_{35}H_{32}F_{30}O_{15}EuZn$): calc.: C, 28.50; H: 2.18. Found: C, 27.83; H, 2.62.

Synthesis of [Gd(hfa)$_2$(tetrag)]$^+$·[Zn(hfa)$_3$]$^-$ (Gd–Zn). Analogously to the previous procedure, 0.89 g (2.2 mmol) of Gd(CH$_3$COO)$_2$·H$_2$O and 0.49 g (2.25 mmol) of Zn(CH$_3$COO)$_3$·xH$_2$O were suspended in 50 ml of dichloromethane, and 0.44 ml of tetraglyme (2.00 mmol) were added. After the addition of 1.41 ml of Hhfa (10 mmol), the suspension was refluxed for 90 minutes under magnetic stirring. After filtration, white crystals were obtained through evaporation of the solvent. The melting point of the obtained compound was 168–170 °C at 760 torr. Elemental analysis ($C_{35}H_{32}F_{30}O_{15}GdZn$): calc.: C, 28.40; H: 2.18. Found: C, 28.20; H, 2.54.

3.3 Characterization

Fourier transform infrared spectra were acquired using a JASCO FT-IR-4600 spectrometer (Easton, MD, USA) in the wavenumber range 4000–400 cm^{-1}. Samples were prepared using complex powders finely ground in an agate mortar with two drops of nujol producing mulls, which was placed between NaCl plates. The instrumental resolution was 4 cm^{-1}. The melting points were measured in air with a Kofler microscope. Elemental analyses were obtained using a EuroVector EA3100 elemental analyzer (CHNS).

Powder X-ray diffraction (PXRD) patterns were recorded using a SmartLab Rigaku diffractometer in the Bragg–Brentano mode, equipped with a rotating anode of Cu K$_\alpha$ radiation operating at 45 kV and 200 mA. The acquisition has been acquired in the 5–30° range with 0.02° incremental step.

Energy dispersive X-ray (EDX) analysis was used to assess the atomic composition of the powders using an INCA-Oxford "windowless" detector with an electron beam energy of 15 keV, with a resolution of 127 eV evaluated as the full width half maximum (FWHM) of Mn K$_\alpha$. The powder were Au-coated before the FE-SEM characterizations in order to ensure a conductive behavior.

UV-Visible spectra were collected by a Shimadzu UV3600 spectrophotometer. Photoluminescence quantum yields, Φ_{lum}, were measured using a C11347 Quantaurus Hamamatsu Photonics K.K Spectrometer. Steady state and time-resolved fluorescence data were obtained using a FLS980 spectrofluorimeter (Edinburg Instrument Ltd).

All EFISH measurements were carried out at the Dipartimento di Chimica of the Università degli Studi di Milano, in $CHCl_3$ solutions at a concentration of 1 × 10^{-3} M, working with a nonresonant incident wavelength of 1.907 μm, obtained by Raman shifting the fundamental 1.064 μm wavelength produced by a Q-switched, mode-locked Nd^{3+}:YAG laser manufactured by Atalaser. The spectrometer for the EFISH measurements was a prototype made by SOPRA (France). The reported $\mu\beta_{EFISH}$ values are the mean of 16 successive measurements performed on the same sample.

Single crystal X-ray diffraction data of **Eu–Zn** were collected, at 100 K, on an Oxford Diffraction Xcalibur diffractometer equipped with a CCD area detector, using Cu-Kα radiation (1.54184 Å), monochromated with a graphite prism. Data were collected and reduced through the CrysAlisPro program.[59] Absorption correction was performed with the ABSPACK program in CrysAlisPro.

The crystal structure was solved using the SIR-2004 package[60] and refined by full-matrix least squares against F^2 using all data (SHELXL-2018/3).[61] All the non-hydrogen atoms were refined with anisotropic displacement parameters. Concerning the hydrogen atoms, all of them were set in calculated positions.

Geometrical calculations were performed by PARST97[62] and molecular plots were produced by the program Mercury (v2025.1.0).[63]

 This journal is © The Royal Society of Chemistry 2026

Table 3 Crystallographic data and refinement parameters for **Eu–Zn**

Empirical formula	$C_{35}H_{27}EuF_{30}O_{15}Zn$
Formula weight	1474.89
T (K)	100
Crystal system, space group	Monoclinic, $P2_1/n$
λ (Å)	1.54184
Unit cell dimensions (Å, °)	a = 14.3630(1)
	b = 23.3155(2), β = 95.113(1)
	c = 15.1258(2)
V (Å^3)	5045.18(9)
Z, d_{calc} (g cm^{-3})	4, 1.942
μ (mm^{-1})	11.017
F(000)	2880
Reflections collected/unique	44 770/9798
Data/parameters	9798/739
Final R indices [$I > 2\sigma(I)$]	R_1 = 0.0406, wR_2 = 0.0871
R indices all data	R_1 = 0.0610, wR_2 = 0.1008
GoF	0.994

Crystallographic data and refinement parameters are reported in Table 3. Complete crystallographic data are available at the Cambridge Crystallographic Data Centre under the CCDC identifier: 2532336.

4. Conclusions

The knowledge of the second-order NLO properties of lanthanide complexes is still very low and, to the best of our knowledge, no cationic lanthanide complex has yet been investigated. This consideration led us to design and synthesize in a simple way two new lanthanide complexes based on a europium cation or gadolinium cation and the same zinc anion: $[Eu(hfa)_2(tetrag)]^+\cdot[Zn(hfa)_3]^-$ and $[Gd(hfa)_2(tetrag)]^+\cdot[Zn(hfa)_3]^-$. Both compounds present $\mu\beta_{EFISH}$ values much higher than that of Disperse Red One, so they are of particular interest for future applications such as in electro-optic modulators. In particular, the gadolinium complex shows a higher $\mu\beta_{EFISH}$ response respect to the europium derivative. The europium complex is luminescent both in solution and in the solid state. The one-step straightforward synthetic procedure represents an added value of these compounds, which are stable in air and obtained starting from commercially available reagents. Furthermore, the synthesis reaches reaction yields over 80% without any further purification. Compositional and structural characterization confirms the formation of cation–anion assemblies, which is resolved with single crystal structure for the **Eu–Zn** adduct. In the future other members of this interesting family of heterobimetallic Ln–Zn complexes will be prepared and studied, in other to get a better understanding of their second-order NLO properties.

Author contributions

Alessia Colombo: investigation, data curation, formal analysis, funding acquisition. Francesco Fagnani and Dominique Roberto: data curation, formal analysis, funding acquisition. Claudia Dragonetti and Anna Lucia Pellegrino: conceptalization, methodology, validation, funding acquisition and writing – supervision and editing and review. Francesca Lo Presti: investigation and data curation. Martina Lippi: investigation. Patrizia Rossi: methodology and validation. Graziella Malandrino: supervision, funding acquisition and review.

Conflicts of interest

There are no conflicts to declare.

Data availability

The data supporting this article have been included as part of the supplementary information (SI). Supplementary information is available. See DOI: https://doi.org/10.1039/d6dt00543h.

CCDC 2532336 contains the supplementary crystallographic data for this paper.[64]

Acknowledgements

The authors thank Bionanotech Research and Innovation Tower (BRIT) laboratory of University of Catania (Grant no. PONa3_00136 financed by the Italian Ministry for Education, University and Research, MIUR) for the diffractometer facility. C. D., A. C., F. F. and D. R. acknowledge The National Interuniversity Consortium of Materials Science and Technology (Project TRI_25_073 Dragonetti and TRI_25_173 Colombo) and the Università degli Studi di Milano (Project PSR2025_DIP_005_GDICA). A. L. P. acknowledges the University of Catania for the Starting Grant "LUMEN" within PiAno di inCEntivi per la Ricerca di Ateneo 2020/2022. C. D., A. C. and D. R. acknowledge Regione Lombardia and cofinanced by European Union– Call "Collabora&Innova" – Project 6154644 – GREEN-TECH – (Applicazione di tecnologie innovative a basso impatto ambientale per lo sviluppo e l'ottimizzazione di processsi chimici sostenibili).

References

1 N. P. Prasad and D. J. Williams, *Introduction to Nonlinear Optical Effects in molecules and Polymers*, Wiley, New York, NY, USA, 1991.
2 D. Lupo, *Molecular Nonlinear Optics: Materials, Physics and Devices*, Academic Press, Boston, MA, USA, 1994.
3 D. R. Kanis, M. A. Ratner and T. J. Marks, *Chem. Rev.*, 1994, **94**, 195–242.
4 L. Beverina, R. Ruffo, G. Patriarca, F. De Angelis, D. Roberto, S. Righetto, R. Ugo and G. A. Pagani, *J. Mater. Chem.*, 2009, **19**, 8190–8197.
5 J. Liu, C. Ouyang, F. Huo, W. He and A. Cao, *Dyes Pigm.*, 2020, **181**, 108509.
6 S. Di Bella, *Chem. Soc. Rev.*, 2001, **30**, 355–366.

7 C. E. Powel and M. G. Humphrey, *Coord. Chem. Rev.*, 2004, **248**, 725.
8 B. J. Coe, Nonlinear Optical Properties of Metal Complexes, in *Comprehensive Coordination Chemistry II*, ed. J. A. McCleverty and T. J. Meyer, Elsevier Pergamon, Oxford, UK, 2004, vol. 9, pp. 621–687.
9 J. P. Morrall, G. T. Dalton, M. G. Humphrey and M. Samoc, *Adv. Organomet. Chem.*, 2007, **55**, 61–136.
10 O. Maury and H. Le Bozec, Metal-based quadratic molecular materials, in *Molecular Materials*, ed. D. W. Bruce, D. O'Hare and R. I. Walton, Wiley, Chichester, UK, 2010.
11 A. Valore, M. Balordi, A. Colombo, C. Dragonetti, S. Righetto, D. Roberto, R. Ugo, T. Benincori, G. Rampinini, F. Sannicolò and F. Demartin, *Dalton Trans.*, 2010, **39**, 10314–10318.
12 A. Colombo, C. Dragonetti, D. Marinotto, S. Righetto, D. Roberto, S. Tavazzi, M. Escadeillas, V. Guerchais, H. Le Bozec, A. Boucekkine and C. Latouche, *Organometallics*, 2013, **32**, 3890–3894.
13 C. Dragonetti, A. Colombo, D. Marinotto, S. Righetto, D. Roberto, A. Valore, M. Escadeillas, V. Guerchais, H. Le Bozec, A. Boucekkine and C. Latouche, *J. Organomet. Chem.*, 2014, **751**, 568–572.
14 A. Colombo, F. Nisic, C. Dragonetti, D. Marinotto, I. P. Oliveri, S. Righetto, M. G. Lobello and F. De Angelis, *Chem. Commun.*, 2014, **50**, 7986–7989.
15 S. Kaur, M. Kaur, P. Kaur, K. Clays and K. Singh, *Coord. Chem. Rev.*, 2017, **343**, 185–219.
16 S. Di Bella, A. Colombo, C. Dragonetti, S. Righetto and D. Roberto, *Inorganics*, 2018, **6**, 133.
17 R. J. Durand, S. Gauthier, S. Achelle, T. Groizard, S. Kahlal, J.-Y. Saillard, A. Barsella, N. Le Poul and F. Robin Le Guen, *Dalton Trans.*, 2018, **47**, 3965–3975.
18 J. M. Cole and C. M. Ashcroft, *J. Phys. Chem. A*, 2019, **123**, 702–714.
19 A. Colombo, C. Dragonetti, V. Guerchais and D. Roberto, *Coord. Chem. Rev.*, 2021, **446**, 214113.
20 H. Belahlou, A. Karakas, K. Waszkowska, A. Gozutok, M. Karakaya, M. Guergouri, A. Bouraiou, S. Bouacida, B. Sahraoui and K. Bouchouit, *Cryst. Growth Des.*, 2023, **23**, 6331–6348.
21 N. Manurkar, M. Ilyas, F. Arshad, P. Patil, Q.-U.-N. Tariq, S. Khan, M. A. Khane and H. Li, *Dalton Trans.*, 2025, **54**, 13443–13458.
22 R. Silpa and N. Palanisami, *J. Phys. Chem.*, 2025, **129**, 17934–17945.
23 M. Muslim, Sultan, L. A. Kamran, Basree, A. K. Pradhan, M. J. Alam, S. M. Afzal, M. Ahmad and M. Afzal, *RSC Adv.*, 2025, **15**, 4657–4668.
24 V. S. Subiksha, P. P. S. Archana and N. Palanisami, *Dalton Trans.*, 2026, **55**, 391–397.
25 R. Marin and D. Jaque, *Chem. Rev.*, 2021, **121**, 1425–1426.
26 G. Malandrino, M. Bettinelli, A. Speghini and I. L. Fragalà, *Eur. J. Inorg. Chem.*, 2001, 1039–1044.
27 A. Picot, A. D'Aléo, P. L. Baldeck, A. Grichine, A. Duperray, C. Andraud and O. Maury, *J. Am. Chem. Soc.*, 2008, **130**, 1532–1533.
28 J. W. Walton, A. Bourdolle, S. J. Butler, M. Soulie, M. Delbianco, B. K. McMahon, R. Pal, H. Puschmann, J. M. Zwier, L. Lamarque, O. Maury, C. Andraudb and D. Parker, *Chem. Commun.*, 2013, **49**, 1600–1602.
29 N. Hamon, M. Galland, M. Le Fur, A. Roux, A. Duperray, A. Grichine, C. Andraud, B. Le Guennic, M. Beyler, O. Maury and R. Tripier, *Chem. Commun.*, 2018, **54**, 6173–6176.
30 N. Hamon, A. Roux, M. Beyler, J.-C. Mulatier, C. Andraud, C. Nguyen, M. Maynadier, N. Bettache, A. Duperray, A. Grichine, S. Brasselet, C.-B. Magali, O. Maury and R. Tripier, *J. Am. Chem. Soc.*, 2020, **142**, 10184–10197.
31 L. A. Galán, N. Hamon, C. Nguyen, E. Molnár, J. Kiss, J. Mendy, K. Hadj-Kaddour, M. Onofre, G. Trencsényi, C. Monnereau, M. Beyler, G. Tircsó, M. Gary-Bobo, O. Maury and R. Tripier, *Inorg. Chem. Front.*, 2021, **8**, 2213–2224.
32 K. Sénéchal, L. Toupet, I. Ledoux, J. Zyss, H. Le Bozec and O. Maury, *Chem. Commun.*, 2004, **19**, 2180–2181.
33 N. Tancrez, C. Feuvrie, I. Ledoux, J. Zyss, L. Toupet, H. Le Bozec and O. Maury, *J. Am. Chem. Soc.*, 2005, **127**, 13474–13475.
34 K. Sénéchal-David, A. Hemeryck, N. Tancrez, L. Toupet, J. A. G. Williams, I. Ledoux, J. Zyss, A. Boucekkine, J.-P. Guégan, H. Le Bozec and O. Maury, *J. Am. Chem. Soc.*, 2006, **128**, 12243–12255.
35 E. Furet, K. Costuas, P. Rabiller and O. Maury, *J. Am. Chem. Soc.*, 2008, **130**, 2180–2183.
36 C. Andraud and O. Maury, *Eur. J. Inorg. Chem.*, 2009, 4357–4371.
37 A. Valore, E. Cariati, S. Righetto, D. Roberto, F. Tessore, R. Ugo, I. L. Fragalà, M. E. Fragalà, G. Malandrino, F. De Angelis, L. Belpassi, I. Ledoux-Rak, K. Hoang Thi and J. Zyss, *J. Am. Chem. Soc.*, 2010, **132**, 4966–4970.
38 G.-L. Law, K.-L. Wong, K.-K. Lau, S.-T. Lap, P. A. Tanner, F. Kuo and W.-T. Wong, *J. Mater. Chem.*, 2010, **20**, 4074–4079.
39 J. W. Walton, R. Carr, N. H. Evans, A. M. Funk, A. M. Kenwright, D. Parker, D. S. Yufit, M. Botta, S. De Pinto and K.-L. Wong, *Inorg. Chem.*, 2012, **51**, 8042–8056.
40 A. Gulino, I. L. Fragalà, F. Lupo, G. Malandrino, A. Motta, A. Colombo, C. Dragonetti, S. Righetto, D. Roberto, R. Ugo, F. Demartin, I. Ledoux-Rak and A. Singh, *Inorg. Chem.*, 2013, **52**, 7550–7556.
41 R. Chakrabarty, A. Dutta, S. Roy, G. Das, I. Ledoux-Rak, P. Mondal, S. K. Prasad, D. S. S. Rao and C. R. Bhattacharjee, *ChemistrySelect*, 2018, **3**, 8245–8251.
42 F. Fagnani, A. Colombo, G. Malandrino, C. Dragonetti and A. L. Pellegrino, *Molecules*, 2022, **27**, 6990.
43 M. Bombaci, F. Lo Presti, A. L. Pellegrino, M. Lippi, P. Rossi, L. Tacconi, L. Sorace and G. Malandrino, *Dalton Trans.*, 2025, **54**, 274–289.
44 K. Clays and A. Persoons, *Phys. Rev. Lett.*, 1991, **66**, 2980–2983.
45 J. Zyss and I. Ledoux, *Chem. Rev.*, 1994, **94**, 77–105.
46 I. Ledoux and J. Zyss, *Chem. Phys.*, 1982, **73**, 203–213.

This journal is © The Royal Society of Chemistry 2026

47 J.-C. G. Bunzli and V. K. Pecharsky, *Handbook on the Physics and Chemistry of Rare Earths: Including Actinides*, Elsevier, Amsterdam, The Netherlands, 2020.
48 S. R. Drake, S. A. S. Miller, M. B. Hursthouse and K. M. A. Malik, *Polyhedron*, 1993, **12**, 1621–1634.
49 P. Van der Sluis, A. L. Spek, K. Timmer and H. A. Meinema, *Acta Crystallogr., Sect. C: Cryst. Struct. Commun.*, 1990, **46**, 1741–1743.
50 N. P. Kuz'mina, A. A. Drozdov, T. V. Zotova, G. N. Kupriyanova, A. P. Pisarevskii and Y. T. Struchkov, *Koord. Khim.*, 1994, **20**, 743.
51 J. A. P. Nash, J. C. Barnes, D. J. Cole-Hamilton, B. C. Richards, S. L. Cook and M. L. Hitchman, *Adv. Mater. Opt. Electron.*, 1995, **5**, 1–10.
52 B.-J. Bae, J. T. Park and I.-H. Suh, *J. Organomet. Chem.*, 2002, **648**, 214–219.
53 C. R. Groom, I. J. Bruno, M. P. Lightfoot and S. C. Ward, *Acta Crystallogr., Sect. B: Struct. Sci., Cryst. Eng. Mater.*, 2016, **72**, 171–179.
54 A. Altomare, N. Corriero, C. Cuocci, A. Falcicchio, A. Moliterni and R. Rizzi, *Cryst. Res. Technol.*, 2015, **50**(9), 696–704.
55 A. A. Coelho, *DIFFRAC.TOPAS V6*, Bruker AXS, Karlsruhe, Germany, 2016.
56 K. Binnemans, *Coord. Chem. Rev.*, 2015, **295**, 1–45.
57 K. D. Singer, J. E. Sohn, L. A. King, H. M. Gordon, H. E. Katz and C. W. Dirk, *J. Opt. Soc. Am. B*, 1989, **6**, 1339–1350.
58 C. W. Dirk, H. E. Katz, M. L. Schilling and L. A. King, *Chem. Mater.*, 1990, **2**, 700–705.
59 *CrysAlisPro, version 1.171.35.19 (release 27-10-2011 CrysAlis171.NET)*, Oxford Diffraction Ltd.
60 M. C. Burla, R. Caliandro, M. Camalli, B. Carrozzini, G. L. Cascarano, L. Da Caro, C. Giacovazzo, G. Polidori and R. Spagna, *J. Appl. Crystallogr.*, 2005, **38**, 381–388.
61 G. M. Sheldrick, *Acta Crystallogr., Sect. C: Struct. Chem.*, 2015, **71**, 3–8.
62 M. Nardelli, *J. Appl. Crystallogr.*, 1995, **28**, 659.
63 C. F. Macrae, I. Sovago, S. J. Cottrell, P. T. A. Galek, P. McCabe, E. Pidcock, M. Platings, G. P. Shields, J. S. Stevens, M. Towler and P. A. Wood, *J. Appl. Crystallogr.*, 2020, **53**, 226–235.
64 CCDC 2532336: Experimental Crystal Structure Determination, 2026, DOI: 10.5517/ccdc.csd.cc2r0385.